Large Molecule Therapeutics

Molecular Cancer Therapeutics

Anetumab Ravtansine: A Novel Mesothelin-Targeting Antibody–Drug Conjugate Cures Tumors with Heterogeneous Target Expression Favored by Bystander Effect

Sven Golfier, Charlotte Kopitz, Antje Kahnert, Iring Heisler, Christoph A. Schatz, Beatrix Stelte-Ludwig, Anke Mayer-Bartschmid, Kerstin Unterschemmann, Sandra Bruder, Lars Linden, Axel Harrenga, Peter Hauff, Frank-Detlef Scholle, Beate Müller-Tiemann, Bertolt Kreft, and Karl Ziegelbauer

Abstract

Mesothelin is a tumor differentiation antigen frequently overexpressed in tumors such as mesothelioma, ovarian, pancreatic, and lung adenocarcinomas while showing limited expression in nonmalignant tissues. Mesothelin is therefore an attractive target for cancer therapy using antibody–drug conjugates (ADC). This study describes the detailed characterization of anetumab ravtansine, here referred to as BAY 94-9343, a novel ADC consisting of a human anti-mesothelin antibody conjugated to the maytansinoid tubulin inhibitor DM4 via a disulfide-containing linker. Binding properties of the anti-mesothelin antibody were analyzed using surface plasmon resonance, immunohistochemistry, flow cytometry, and fluorescence microscopy. Effects of BAY 94-9343 on cell proliferation were first studied *in vitro* and subsequently *in vivo* using subcutaneous, orthotopic, and patient-derived xenograft tumor models. The antibody binds to human mesothelin with high affinity and selectivity, thereby inducing efficient antigen internalization. *In vitro*, BAY 94-9343 demonstrated potent and selective cytotoxicity of mesothelin-expressing cells with an IC_{50} of 0.72 nmol/L, without affecting mesothelin-negative or nonproliferating cells. *In vivo*, BAY 94-9343 localized specifically to mesothelin-positive tumors and inhibited tumor growth in both subcutaneous and orthotopic xenograft models. In addition, BAY 94-9343 was able to induce a bystander effect on neighboring mesothelin-negative tumor cells. Antitumor efficacy of BAY 94-9343 correlated with the amount of mesothelin expressed and was generally superior to that of standard-of-care regimen resulting in complete tumor eradication in most of the models. BAY 94-9343 is a selective and highly potent ADC, and our data support its development for the treatment of patients with mesothelin-expressing tumors. *Mol Cancer Ther; 13(6); 1537–48. ©2014 AACR.*

Introduction

Mesothelin, a glycosylphosphatidylinositol (GPI)-anchored glycoprotein, is highly overexpressed in several human tumors, including the majority of ovarian and pancreatic adenocarcinomas, and in 100% of epithelial mesotheliomas. Moreover, mesothelin expression is found in 50% of lung adenocarcinomas, 60% of gastric cancers, and 67% of triple-negative breast cancers (1–8). Expression in normal tissues is mainly restricted to the single cell layers lining the pleura, pericardium, and peritoneum (1, 9).

There is currently limited information available on the physiologic function of mesothelin. Mesothelin-deficient mice are fertile and do not exhibit any apparent phenotype (10). Mesothelin is known to bind to CA125 (cancer antigen 125, also known as MUC16), and this interaction may be involved in the metastatic spread of CA125-expressing ovarian cancer cells that bind to mesothelin-expressing cells lining the peritoneal cavity (11, 12). Mesothelin may further contribute to metastasis by inducing the expression of matrix metalloproteinases 7 and 9 (13, 14). In pancreatic cancer cells, mesothelin has been shown to contribute to tumorigenesis by inducing interleukin-6 expression and cell proliferation and by promoting resistance to TNF-α (15, 16). Because of high expression in several cancers and a conversely restricted expression in normal tissues, mesothelin is an attractive target for anticancer therapy.

Preclinical and clinical development of naked antibodies and recombinant immunotoxins targeting mesothelin has

Authors' Affiliation: Bayer HealthCare Pharmaceuticals, Berlin/Wuppertal, Germany

Note: Supplementary data for this article are available at Molecular Cancer Therapeutics Online (http://mct.aacrjournals.org/).

S. Golfier and C. Kopitz contributed equally to this work.

Corresponding Author: Sven Golfier, Bayer HealthCare Pharmaceuticals, Muellerstr 178, 13353 Berlin, Germany. Phone: 49-30-468192707; Fax: 49-30-468992707; E-mail: sven.golfier@bayer.com

doi: 10.1158/1535-7163.MCT-13-0926

been reported (17). MORAb-009 (amatuximab), a chimeric anti-mesothelin monoclonal antibody, SS1P, a recombinant anti-mesothelin immunotoxin, and CRS-207, a live-attenuated Listeria vaccine expressing mesothelin engineered for targeted elimination of mesothelin-expressing cells, are all in clinical trials (18–20). The nonhuman origin renders recombinant immunotoxins highly immunogenic inducing the generation of neutralizing antibodies and thereby preventing multiple treatments. For instance, SS1P showed only limited antitumor activity because most patients developed neutralizing antibodies against the drug (21). Therefore, less immunogenic variants are being evaluated (22). Alternatively, mesothelin can be targeted with antibody–drug conjugates (ADC) combining the specificity of an antibody with the potency of a toxophore. Antibodies conjugated to various toxophores have shown potent antitumor activity in preclinical animal models (23). Recently, encouraging clinical efficacy has been observed with SAR3419 targeting CD19 (24). Furthermore, approvals of brentuximab vedotin targeting CD30 (25, 26) and trastuzumab-DM1 in HER2-positive breast cancer (27–29) support the development of ADCs for cancer treatment.

Herein, we introduce a novel ADC, BAY 94-9343, consisting of a fully human anti-mesothelin antibody (MF-T) coupled via a reducible disulfide linker to a microtubule-targeting toxophore DM4. This combination of a linker and toxophore was selected because of its reported potential bystander effect (30). According to detailed preclinical characterization both *in vitro* and *in vivo*, BAY 94-9343 is highly selective and shows strong *in vivo* efficacy in several pancreatic and ovarian cancers and in mesothelioma models, including patient-derived xenografts.

Materials and Methods

Cells

CHO-K1, MIA PaCa-2, and OVCAR-3 cells were obtained from the American Type Culture Collection, NCI-H226 cells from NIH (Rockville, MA), and HT-29 from DSMZ. All cell lines, excluding CHO-K1, were authenticated using PCR fingerprinting by the provider. Cells were maintained in an incubator of 5% CO_2 at 37°C. NCI-H226 cells were cultured in RPMI-1640 with 10% fetal calf serum (FCS) and 2 mmol/L glutamine; OVCAR-3 cells in RPMI-1640 with 20% FCS, 10 μg/mL insulin (bovine), and 2 mmol/L glutamine; HT-29 cells in RPMI-1640 with 10% FCS, 1% sodium bicarbonate, and 2% hygromycin; and MIA PaCa-2 cells in DMEM/HAMS F12 with 10% FCS, 2.5% horse serum, and 2 mmol/L glutamine. Human adult mesothelial cells, obtained from Zen-Bio, were cultured according to the provider's instructions.

Preparation of mesothelin-expressing cell lines

CHO-K1 cells were stably transfected with a pEAK vector (31) encoding the GPI-anchored, N-terminally FLAG-tagged mesothelin protein and selected with puromycin to give a CHO-A9 mesothelin-expressing cell line. HT-29 and MIA PaCa-2 cells were transfected with pcDNA3.1Hyg without (vector control) and with human mesothelin cDNA (including flag tag), using Lipofectamine 2000 (Invitrogen). Cells were selected with hygromycin for 2 weeks and subcloned by limiting dilution, and stable transfectants were generated. Mesothelin expression was assessed by fluorescence-activated cell sorting (FACS; FC500, Beckman-Coulter) using MF-T and a fluorescein isothiocyanate (FITC)-conjugated anti-human immunoglobulin G (IgG) secondary antibody (Sigma). The resulting cell lines were HT29/vector, HT29/meso, MIA PaCa-2/vector, and MIA PaCa-2/meso (MIA PaCa-2#37; overexpressing mesothelin).

Preparation and characterization of mesothelin antibody MF-T and ADC BAY 94-9343

Mesothelin antibody discovery using the HuCAL Gold Fab-phage library, the expression, purification, and characterization of Fab and IgG are described in Supplementary Methods. MF-T was conjugated to the maytansinoid DM4 via a hindered disulfide linker (SPDB) at ImmunoGen, following published procedures (32–34). An average drug to antibody ratio of 3.2 was achieved, which is in agreement with the previously described optimal range of 2 to 4 (35). Because different batches of BAY 94-9343 were used, the doses were calculated on the basis of the amount of DM4, the toxic proportion of the antibody. The used doses calculated on the basis of the total ADC are indicated in brackets. Calibrated FACS analysis and immunohistochemistry (IHC) of the cells and tumor sections and the antibody internalization assay are described in Supplementary Methods.

In vivo tumor targeting

MF-T antibody was conjugated with a Bayer HealthCare proprietary near infrared (NIR)-fluorescent tetrasulfonated carbocyanine dye, and fluorescence imaging was performed as previously described (36). Briefly, 12 NMRI *nu/nu* mice (Taconic M&B A/S Breeding) per group were subcutaneously inoculated with 1×10^6 HT-29/meso or HT29/vector cells suspended in 0.1 mL 50% Matrigel (BD Biosciences). Before imaging, all animals received a single intravenous injection of fluorescent dye-conjugated MF-T.

Proliferation assay

To determine IC_{50} of cell viability, 0.8×10^3 cells/well were seeded in 384-well plates, incubated for 24 hours, and thereafter washed with $PBS^{Ca+,Mg+}$ and treated with 0.01 to 300 nmol/L BAY 94-9343. After 4 or 24 hours, the cells were washed with $PBS^{Ca+,Mg+}$, and growth medium was added. The proliferation assay endpoint was selected on the basis of the observation that ADC internalization is saturated by 24 hours (Fig. 2D). The plates were incubated for 72 or 92 hours, and cell proliferation was quantified using the WST-1 assay (Roche) according to the manufacturer's instructions with the following exception: 5 μL (instead of 10 μL) WST-1 mixture was added into each well. IC_{50} was assessed using the Prism 4 software (GraphPad Software), setting the positive control (untreated

cells) at 100% and the negative control (without cells) at 0%.

In vivo tumor models

All animal experiments were conducted in accordance with the German animal welfare law and approved by local authorities. For subcutaneous tumor models, female NMRI *nu/nu* mice (18–25 g, 7–10 weeks) from Taconic M&B were implanted on day 0 with either 3×10^6 MIA PaCa-2/vector, 3×10^6 MIA PaCa-2/meso, 1×10^6 HT-29/vector, 1×10^6 HT-29/meso, 3×10^6 OVCAR-3, or 3×10^6 NCI-H226 cells suspended in 0.1 mL 50% Matrigel. Patient-derived pancreatic (PAXF736) model was performed at Oncotest GmbH and ovarian (OVCAR6719) and mesothelioma (Meso7212) models at EPO Berlin-Buch GmbH. Tumor fragments were subcutaneously passaged on naïve female NMRI *nu/nu* (5–7 weeks, Charles River; PAXF736), naïve NOD SCID (8 weeks, Taconic M&B; OVCAR6719), or naïve male NMRI *nu/nu* (Charles River; Meso7212) mice as previously described (37). Subcutaneous tumor growth was monitored by measuring the tumor volume [(length $\times$ width^2)/2]. Treatment response was defined using the Response Evaluation Criteria in Solid Tumors (RECIST) criteria. Partial regression (PR) was defined as more than 30% reduction in tumor size and tumor eradication as an absence of any palpable tumor mass. No tumor growth or a slight (< 30%) reduction or a slight (< 20%) increase in tumor size was defined as a stable disease.

For the orthotopic ovarian cancer model, NMRI *nu/nu* mice were anesthetized [intraperitoneal (i.p.) administration of 80 mg/kg ketamine (Pfizer) and 16 mg/kg xylazine (Bayer HealthCare AG)]. An incision was made in the dermis and peritoneum on the left side near the backbone, the ovary was exteriorized and injected with 1.5×10^6 OVCAR-3-s-05 cells (OVCAR-3 cells stably transfected with luciferase), suspended in 15 μL of 100% Matrigel. The ovary was then replaced and the incision clamped with wound clips. The mice were subcutaneously implanted with 17β-estradiol-pellets (0.36 mg/pellet, 60-day release, Innovative Research of America). Analgesia (carprofen, 5 mg/kg, s.c.) was used on the evening before surgery, directly before anesthesia, and daily after surgery for a total of 3 days. Tumor growth was monitored by bioluminescence imaging (BLI). Mice received intravenous (i.v.) D-Luciferin Sodium Salt (Synchem OHG, 100 μL 45 mg/mL in PBS) and were anesthetized with 3% isofluran. Anesthesia was maintained with a mixture of oxygen: nitrous oxide: isofluran (0.1 L/minute : 0.05 L/minute : 2%, respectively). Photon release by oxy-luciferin was detected using NightOWL (Berthold Technologies). At the end of the study, the ovaries were harvested and weighed.

Mice were administered intravenously with BAY 94-9343, a nontargeted isotype control ADC BAY 86-1899, MF-T, or S-methyl-DM4 on days 5, 8, and 12 (mice implanted with MIA PaCa or HT29 meso cells); on days 33, 36, and 40 (OVCAR-3); on days 78, 81, 84, 127, 130, and 133 (NCI-H226); on days 15, 18, and 22 (OVCAR-3-s-05 orthotopic); on days 7, 10, and 13 (HT29 titration); Q3Dx3 starting on day 0 (PAXF736); Q3Dx3 starting on day 29 (OVCAR6719); or Q4Dx3 starting on day 34 (Meso7212) after tumor cell inoculation. The doses of BAY 94-9343 and isotype control BAY 86-1899 indicated in the text and figures of the efficacy experiments refer to the amount of DM4 in the ADC (0.2 mg/kg DM4 corresponds to 10 mg/kg ADC). The vehicle was 10 mmol/L histidine, 130 mmol/L glycine, 5% (w/v) sucrose, pH 5.5. Cisplatin (Sigma-Aldrich or Hexal, 3 mg/kg unless otherwise stated, i.p), pemetrexed (Lilly Pharma, 100 mg/kg, i.p.), gemcitabine (Lilly Pharma, 240 mg/kg, i.p.), and vinorelbine (Hexal, 5 mg/kg, i.p.) were used as standard-of-care compounds in respective models. In the NCI-H226 model, cisplatin was administered Q3D between days 78 and 117 with a 6-day resting period between days 90 and 96. In the combination group, cisplatin (Q3D) was administered until day 117 with a 6-day resting period between days 90 and 96, and four cycles of pemetrexed (all Q1Dx7) were administered with 8, 11, and 12-day resting periods between the cycles, respectively. The final doses were given on day 130 for cisplatin and 137 for pemetrexed. In the PAXF736 model, gemcitabine was administered Q1Wx3 starting on day 0. In the OVCAR6719 model, cisplatin (6 mg/kg) was given on days 29 and 36. In the Meso7212 model, cisplatin (Q3D) was administered between days 34 and 70, pemetrexed Q1Dx7 with 7-day resting periods (two and half cycles) between days 34 and 64, and vinorelbine Q1Wx5 between days 34 and 62. Dose volume of 10 mL/kg body weight was used, and intravenous administration was performed *via* tail vein injection.

Statistical analyses

Statistical analyses for the comparison of more than two groups were performed by one-way ANOVA, followed by a Dunnett test (comparisons against one group) or Bonferroni test (pairwise comparisons). Two-group comparisons were performed by Student *t* test. *P* values less than 0.05 were considered statistically significant.

Results

Mesothelin expression in cancer

The eligibility of mesothelin for antibody-directed drug targeting was confirmed in a set of tumor samples with high prevalence of mesothelin overexpression, that is, mesothelioma, ovarian, and pancreatic cancer (Supplementary Fig. S1 and Supplementary Table S1). On the basis of comparative immunohistochemical analyses of primary and metastatic ovarian cancer samples, obtained from the same patient, mesothelin expression remained mostly stable or increased during disease progression in 86% of the cases (Fig. 1A). Concordant with published data (38), the highest endogenous mesothelin expression was found in OVCAR-3 cells (24,000 antibodies bound per cell) as measured by

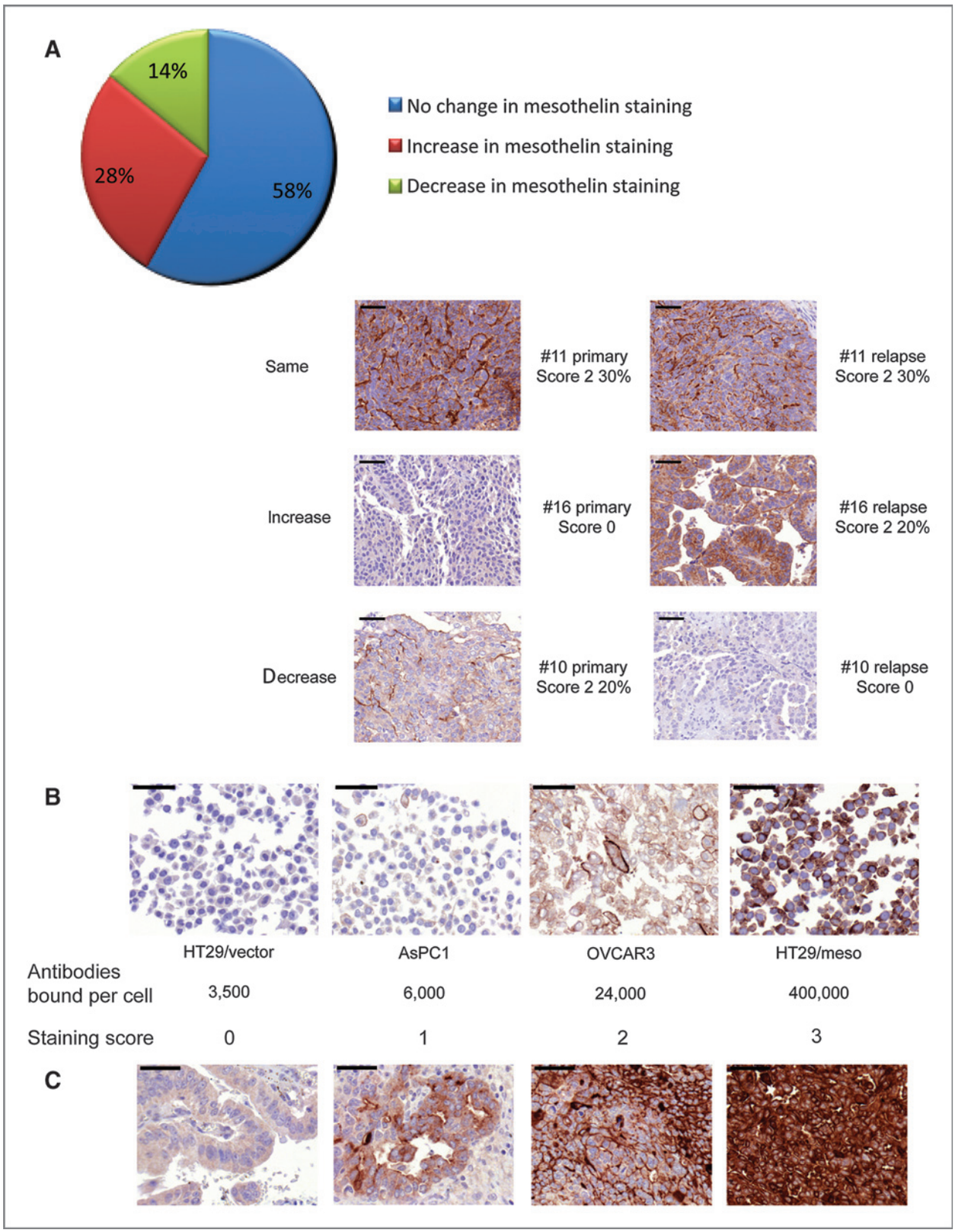

Figure 1. Mesothelin expression in clinical samples and cell lines. A, change in mesothelin staining intensity in primary ovarian cancer samples versus matched relapse ($n = 50$). B, immunohistochemical staining of cell lines for which the number of antibodies bound per cell was determined by quantitative FACS analysis. C, immunohistochemical staining of primary ovarian cancer samples. Quantification of staining (staining score) is based on the staining intensity of the cell lines. Scale bar, 50 μm.

calibrated IHC (Fig. 1B). In comparison with the endogenous expression in cancer cell lines, mesothelin expression was much higher in primary ovarian cancer samples (Fig. 1B and C).

Preparation and characterization of a mesothelin ADC (BAY 94-9343)

To generate a mesothelin-specific ADC, 22 unique mesothelin-binding Fab sequences were identified using MorphoSys HuCAL technology (39), and selected Fabs were converted to human IgG1s. The MF-T Fab sequence was selected because of a high binding affinity for human mesothelin (Kd of 10 nmol/L) detected by surface plasmon resonance (SPR) and due to identical staining of HT29/meso xenograft tumor sections (Fig. 2A) and primary human cancer samples (Fig. 2B) compared with mesothelin control antibodies. Moreover, flow-cytometric binding curves for MF-T and endogenous mesothelin-expressing NCI-H226 cells showed a sigmoid increase in the fluorescence signal, characteristic for specific antibody binding (Fig. 2C). MF-T was found not to bind to mouse, rat, or monkey mesothelin, confirmed by SPR (data not shown) and IHC (Supplementary Figs. S2–S4).

A prerequisite for ADC activity is its internalization upon target binding, to effectively deliver the cytotoxic payload into the cells. To study MF-T internalization, MF-T was labeled with a pH-sensitive fluorescent dye CypHer5E exhibiting fluorescence activity at acidic pH, that is, in late endosomes and lysosomes (40). Consequently, any detected fluorescent signal is derived from internalized antibodies. In OVCAR-3 cells, MF-T internalization was enhanced by >2.5-fold as compared with the unspecific internalization of the isotype control, with maximal differences observed during the first 3 hours of incubation (~4-fold; Fig. 2D).

The therapeutic function of an ADC is highly dependent on the specific intracellular delivery of toxophores to target presenting cells. Therefore, we next studied the ability of MF-T to selectively accumulate in mesothelin-positive tumors *in vivo*. Because MF-T showed no cross-reactivity with murine mesothelin, the target in this approach is comprised by the inoculated tumor only. Fluorescently-labeled MF-T was injected into mice bearing either HT29/meso or HT29/vector tumors. NIR fluorescence imaging revealed that MF-T accumulation in HT29/meso tumors was 1.4-fold higher than in HT29/vector tumors (Fig. 2E).

As MF-T demonstrated the desired properties of an effective ADC antibody, we subsequently linked MF-T to an average of 3.2 DM4 molecules through a disulfide linker to produce the ADC BAY 94-9343. Importantly, conjugation with DM4 did not alter the binding properties of MF-T as demonstrated by SPR analysis (data not shown) and IHC (Fig. 2A).

Cytotoxicity of BAY 94-9343 *in vitro*

Next, we determined IC_{50} values for BAY 94-9343 in human pancreatic (MIA PaCa-2) and colon carcinoma (HT-29) cell lines, transfected with human mesothelin or the corresponding vector control, and in human ovarian carcinoma (OVCAR-3) and mesothelioma (NCI-H226) cell lines with endogenous mesothelin expression. BAY 94-9343 showed antiproliferative activity with IC_{50} in the low nanomolar range with respect to antibody concentration in all of the mesothelin-expressing tumor cell lines tested (Fig. 3A–D). In contrast, mesothelin-negative tumor cells were not affected by BAY 94-9343 except at very high concentrations approaching the micromolar range (Fig. 3A and B). In accordance with DM4 mode of action, that is, inhibition of microtubule dynamics, BAY 94-9343 did not affect nondividing mesothelin-positive primary peritoneal mesothelial cells (Fig. 3E). Mesothelin expression in these cell types was confirmed by IHC or FACS analysis (Supplementary Fig. S5).

Antitumor activity of BAY 94-9343 *in vivo*

We evaluated the antitumor activity of BAY 94-9343 *in vivo*. The highest dose and schedule selected for the studies, 0.2 mg/kg based on the amount of DM4 (corresponding to 9.5–14.3 mg/kg ADC, depending on the antibody to drug ratio in the respective ADC batch), did not affect mouse body weight. In the *xenogeneic* tumor models MIA PaCa-2/meso or HT-29/meso cells, BAY 94-9343 showed dose-dependent efficacy, and treatment with 0.2 mg/kg (10.6 mg/kg ADC) BAY 94-9343 resulted in complete tumor eradication, lasting for at least 17 weeks following the final treatment (Fig. 4A–C and Supplementary Fig. S6A). At a dose of 0.05 mg/kg (2.7 mg/kg ADC), BAY 94-9343 eradicated tumors in 5 out of 6 animals in the MIA PaCa-2/meso pancreatic cancer model (Fig. 4A and B), whereas in the HT-29/meso colon cancer model, tumor regression without complete eradication was observed in 25% of the animals ($P < 0.001$; Fig. 4C). Treatment with unconjugated MF-T in the pancreatic tumor model (data not shown) or with free S-methyl-DM4 in the colon cancer model did not significantly affect tumor growth (Fig. 4C). Treatment of HT-29/meso tumors with 0.2 mg/kg BAY 86-1899 (corresponding to 9.5 mg/kg ADC), a nontargeted isotype control ADC, reduced tumor size by 73% as compared with the vehicle control. However, in contrast with BAY 94-9343, BAY 86-1899 did not result in tumor eradication and lower doses did not significantly affect tumor growth (Fig. 4C).

Next, we studied whether BAY 94-9343 shows antitumor activity in endogenous mesothelin-expressing tumor models. In the *xenogeneic* OVCAR-3 ovarian cancer model treated with 0.05 mg/kg (Q3Dx3) BAY 94-9343 (2.8 mg/kg ADC), 100% of mice responded to the treatment, and complete tumor eradication was observed in 4 out of 6 mice lasting for at least 12 weeks following the final treatment. In contrast, the ADC isotype control reduced tumor growth at a dose of 0.2 mg/kg (9.5 mg/kg ADC) compared with the vehicle but did not have any effect at the comparatively lower dose used for BAY 94-9343 (0.05 mg/kg; 2.4 mg/kg ADC; Fig. 4D and Supplementary

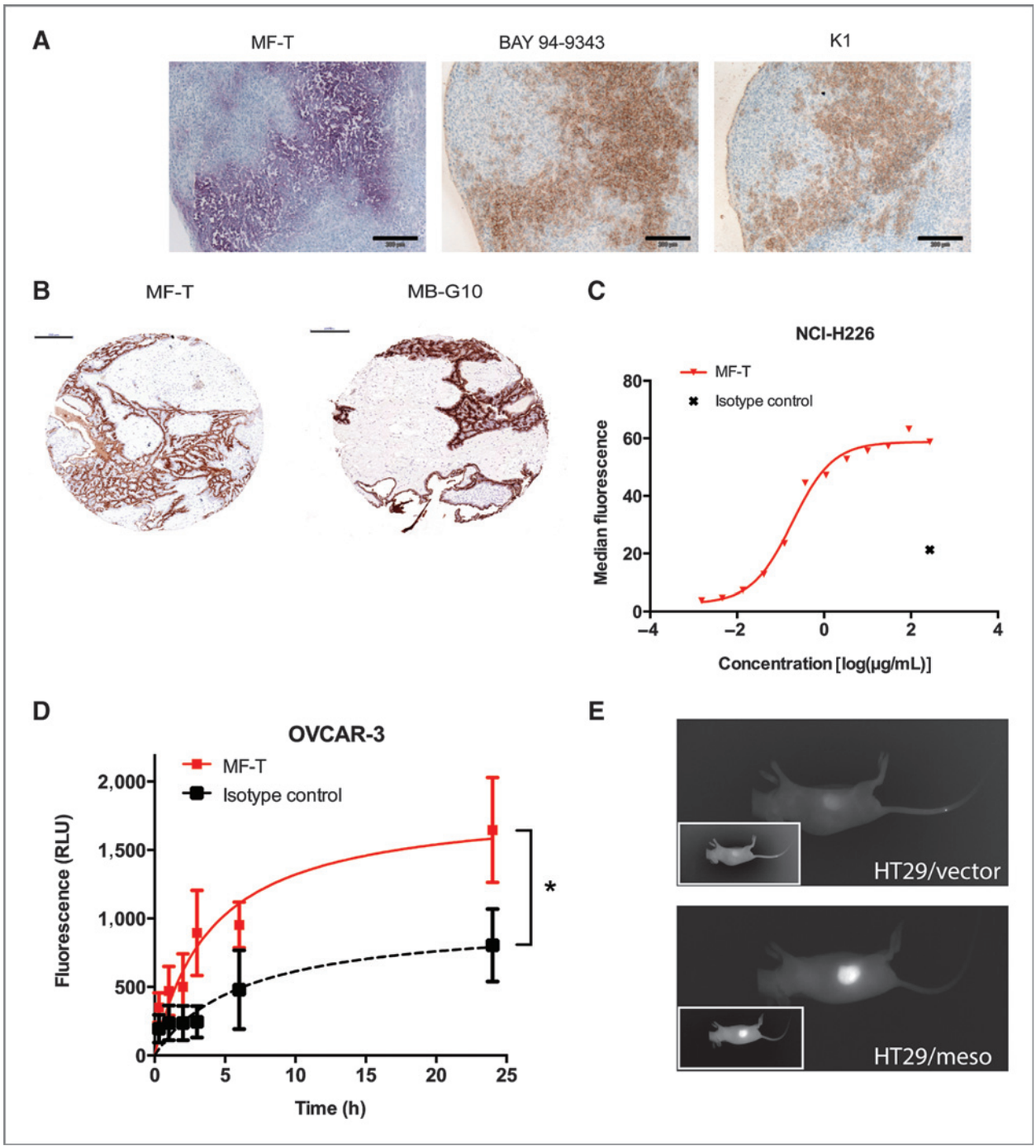

Figure 2. Mesothelin binding, internalization, and *in vivo* targeting properties of MF-T and BAY 94-9343. A, immunohistochemical staining of consecutive MIA PaCa-2/meso xenograft sections. Mesothelin expression was detected by MF-T, BAY 94-9343, and monoclonal murine antibody K1. Scale bar, 50 µm. B, immunohistochemical staining of two sections of an ovarian cancer sample. Mesothelin expression was detected by MF-T and monoclonal murine antibody MB-G10. Scale bar, 200 µm. C, antibody titration of MF-T results in sigmoid increase in the FACS signal for mesothelin-positive NCI-H226 cells, characteristic for specific antibody binding. D, OVCAR-3 cells were incubated with CypHer5E dye-labeled MF-T or isotype control and the relative fluorescence signal (mean ± SD) was measured over time. *, $P < 0.05$. E, representative images of HT29/meso and HT29/vector tumor-bearing mice injected with tetrasulfonated carbocyanine dye-labeled MF-T. Fluorescence was imaged 168 hours after injection.

Fig. S6B). In the NCI-H226 mesothelioma model, two Q3Dx3 cycles of BAY 94-9343 were applied and compared with the standard therapy cisplatin and to the combination of cisplatin and pemetrexed. The dose of 0.2 mg/kg (11.2 mg/kg ADC) BAY 94-9343 inhibited tumor growth by 94% as compared with the vehicle control on day 153

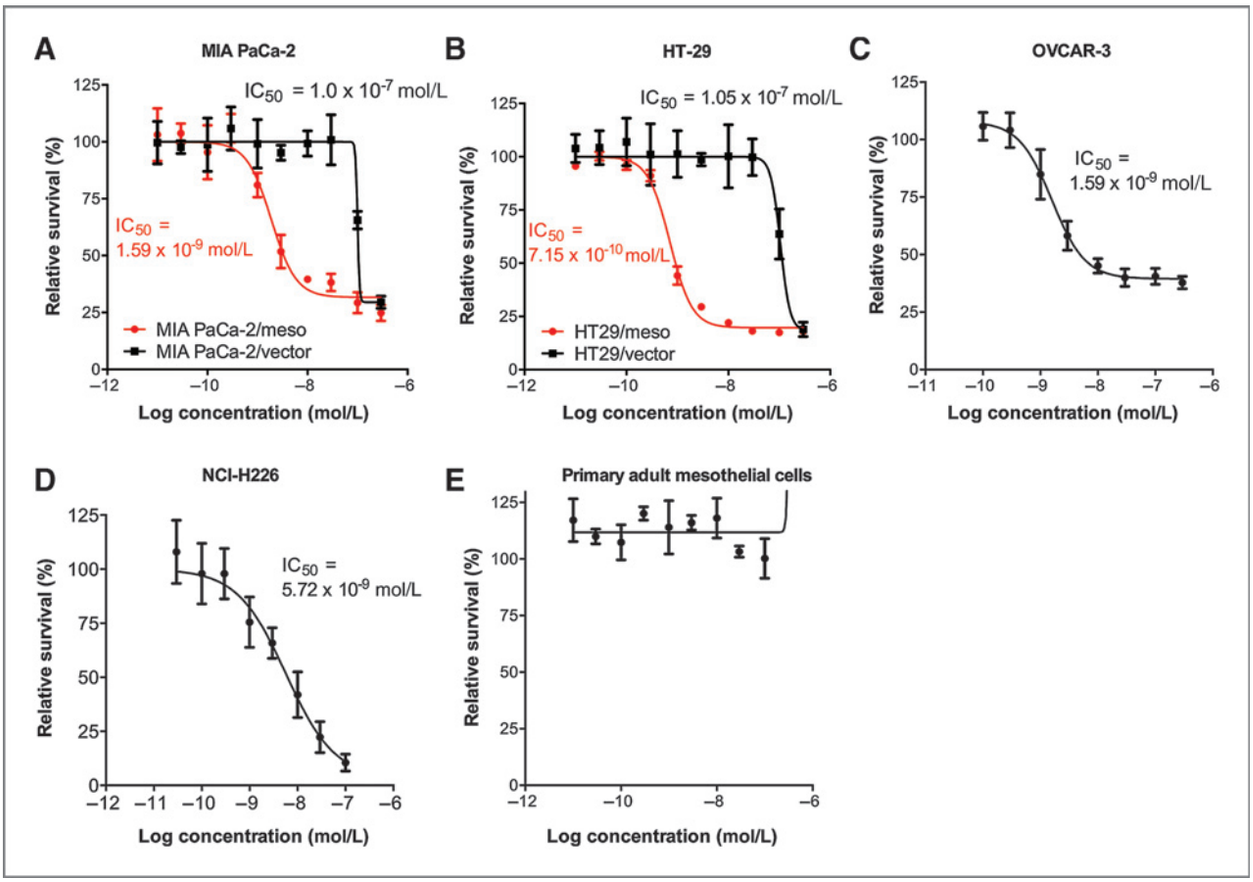

Figure 3. Cytotoxicity of BAY 94-9343 *in vitro*. Survival (mean ± SD) of mesothelin or vector control transfected tumor cell lines MIA PaCa-2 (A) and HT-29 (B), NCI-H226 (C), and OVCAR-3 (D), and primary adult mesothelial cells (E) in response to different concentrations of BAY 94-9343. Concentration values are presented in terms of antibody concentration.

($P < 0.001$) and achieved a 63% response rate (partial regression in 5 out of 8 mice), whereas cisplatin alone and in combination with pemetrexed resulted in 70% reduction of tumor growth ($P < 0.01$; Fig. 4E and Supplementary Fig. S6C). The treatment groups were also compared by measuring the tumor weight at the end of the study (day 174). Two treatment cycles with 0.2 mg/kg (11.2 mg/kg ADC) BAY 94-9343 resulted in a 14-fold lower tumor weight as compared with the combination of cisplatin and pemetrexed ($P < 0.05$; Supplementary Fig. S6D).

The inhibitory effect of BAY 94-9343 on tumor growth was also analyzed in an orthotopic ovarian cancer model using endogenous mesothelin-expressing human ovarian cancer cells (OVCAR-3-s-05). Treatment with 0.2 mg/kg (10.6 mg/kg ADC; Q3Dx3) BAY 94-9343 markedly reduced tumor burden as indicated by 81% reduction in ovary weight at the end of the study as compared with the vehicle treatment ($P < 0.05$). Neither the control ADC BAY 86-1899 (0.2 mg/kg based on DM4, corresponding to 9.5 mg/kg ADC) nor unconjugated S-methyl-DM4 alone or in combination with MF-T significantly affected tumor growth (Fig. 4F and G).

Antitumor activity of BAY 94-9343 in patient-derived tumor models

Tumor models based on established tumor cell lines have the disadvantage of low heterogeneity (37). Therefore, we used tumor models based on the transfer and *in vivo* passage of human patient-derived tumors in immunocompromised mice. BAY 94-9343 administered at 0.2 mg/kg (corresponding to 14.3 mg/kg ADC; Q3Dx3) resulted in transient regression in 6 out of 8 tumors in the pancreatic tumor model PAXF736 ($P < 0.001$; Fig. 5A), complete eradication of the ovarian tumor OVCAR6719 in all mice ($P < 0.001$; Fig. 5B), and at least partial tumor regression in all mice in the mesothelioma model Meso7212 ($P < 0.001$; Fig. 5C). Comparisons of respective standards of care revealed that the antitumor efficacy of BAY 94-9343 was more pronounced than gemcitabine ($P < 0.01$) in the pancreatic model, cisplatin ($P < 0.01$) in the ovarian model, and cisplatin ($P < 0.05$) and pemetrexed ($P < 0.001$) in the mesothelioma model. The difference between the effects of a microtubule-targeting drug vinorelbine and BAY 94-9343 in the mesothelioma model was not significant (Fig. 5).

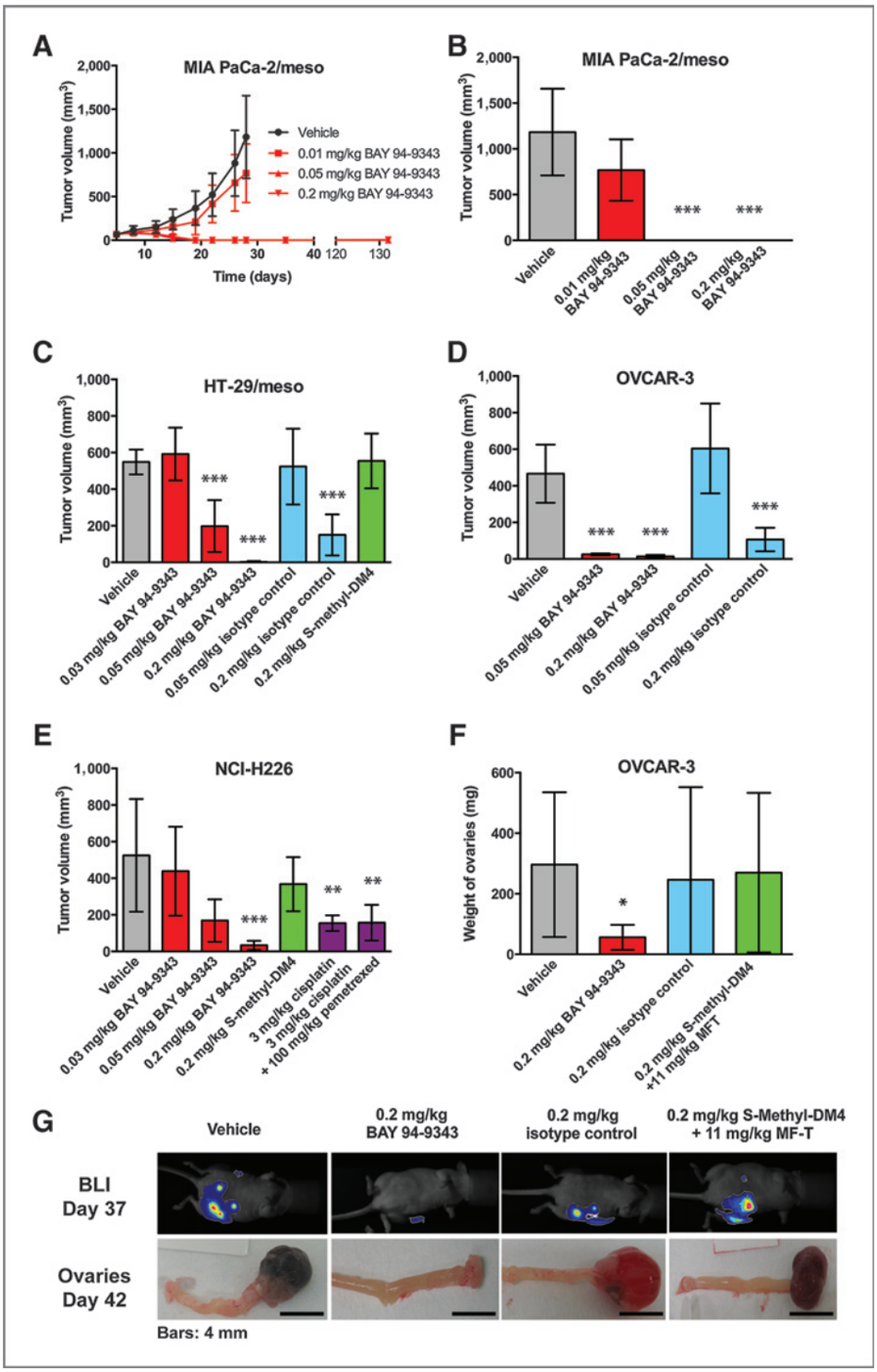

Figure 4. Antitumor activity of BAY 94-9343 *in vivo*. MIA PaCa-2/meso, HT-29/meso, OVCAR-3, and NCI-H226 tumors were grown subcutaneously (A–E) and OVCAR-3-s-05 orthotopically in the ovary (F–G) in nude mice. Mice were randomized into treatment groups (MIA PaCa-2/meso and OVCAR-3, $n = 6$; HT-29/meso and NCI-H226, $n = 8$; OVCAR-3-s-05, $n = 9$) when tumors were measurable by caliper (A–E), or BLI was performed to exclude tumor-free mice before randomization (F–G). A, mean ± SD of tumor volume in MIA PaCa-2/meso tumor model over time. B–E, mean ± SD of tumor volume of MIA PaCa-2/meso on study day 28 (B), HT-29/meso on study day 21 (C), OVCAR-3 on study day 61 (D), and NCI-H226 on study day 153 (E). F, weight of ovaries (mean ± SD) on day 42. Orthotopically inoculated mice were treated on days 15, 18, and 22 after tumor cell inoculation. G, representative BLI images of tumors *in situ* on day 37 and harvested ovaries on day 42. *, $P < 0.05$; **, $P < 0.01$; ***, $P < 0.001$, as compared with the vehicle control.

Titration of mesothelin-positive tumor cells *in vivo*

To determine the minimum proportion of mesothelin-positive cells required for BAY 94-9343-mediated tumor response, different ratios of mesothelin-positive HT-29/meso and mesothelin-negative HT-29/vector cells were subcutaneously inoculated into nude mice, resulting in tumors with 100%, 80%, 60%, 20%, and 0% mesothelin-positive cells (Fig. 6A). Treatment of these tumors demonstrated a pronounced mesothelin expression-dependent antitumor efficacy of 0.2 mg/kg BAY 94-9343 (corresponding to 11.2 mg/kg ADC; Fig. 6B). In tumors with 100% mesothelin-positive cells, complete tumor

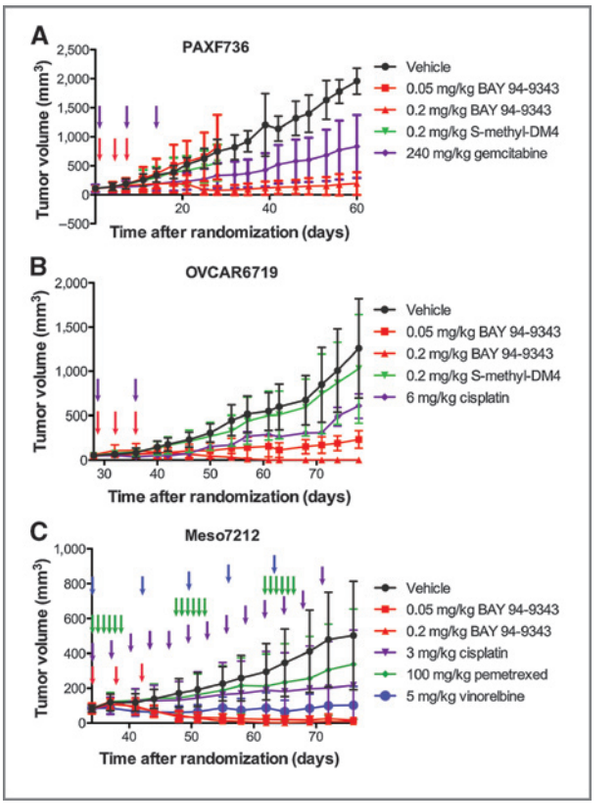

Figure 5. Antitumor activity of BAY 94-9343 in patient-derived tumor models. Fragments of human tumors were passaged in naïve immunocompromised mice. After randomization into groups, treatments (BAY 94-9343 and S-methyl-DM4 i.v., gemcitabine i.p., cisplatin i.p.) were initiated (time points indicated by arrows). Mean ± SD of tumor volume for the pancreatic cancer model PAXF736 ($n = 9$; A), ovarian cancer model OVCAR6719 ($n = 8$; B), and mesothelioma model Meso7212 ($n = 10$; C).

regression was achieved in 7 out of 8 mice (data not shown) and in three of the cases, regression was observed as early as 28 days when the vehicle control group was sacrificed (Fig. 6B). Furthermore, a 100% response rate to the BAY 94-9343 treatment was observed even in tumors with 40% mesothelin expression. In the 20% mesothelin-positive group, the treatment reduced mean tumor size by 82% compared with the vehicle, and tumor size remained either the same or reduced in 7 out of 8 mice (4 stable disease, 3 PR). In contrast, tumor size was increased by 30% to 300% in 7 out of 8 mice bearing mesothelin-negative tumors treated with BAY 94-9343. However, tumor size was approximately 64% smaller in this group as compared with the vehicle, demonstrating a small target-independent antitumor effect at this dose (0.2 mg/kg based on DM4, corresponding to 11.2 mg/kg ADC; Q3Dx3).

Discussion

A high medical need remains for the treatment of advanced mesothelioma, pancreatic, and recurrent ovarian cancers. A large proportion of these tumors have been shown to overexpress the surface protein mesothelin. Moreover, the limited expression of mesothelin in normal human tissues qualifies mesothelin as an attractive candidate for antibody-based cancer therapy. This study describes the establishment of human anti-mesothelin antibody MF-T conjugated to the tubulin inhibitor DM4 and includes detailed preclinical characterization of the resulting BAY 94-9343, an ADC targeting mesothelin-expressing tumors.

The overexpression of mesothelin in mesothelioma, ovarian and pancreatic cancer specimens was confirmed by detailed immunohistochemical studies. More importantly, it was demonstrated for the first time that mesothelin continues to be expressed in recurrent ovarian cancer in most patients, suggesting that immunohistochemical staining of archived primary tumor biopsies could be used to stratify patients for anti-mesothelin therapy.

The efficacy of unconjugated antibodies relies on the function of their target antigen as demonstrated by the growth factor receptor blocking activity exhibited by antibodies such as cetuximab and trastuzumab for EGF receptor and HER2/neu, respectively (41, 42). The unknown biologic function of mesothelin does not, however, conflict with the development of an ADC. The efficacy of an ADC predominantly depends on the expression of the target antigen, ADC-binding affinity and subsequent internalization within the cells, and the potency of the conjugated toxophore. Our data demonstrate that the MF-T antibody possesses a specific nanomolar-binding affinity for human mesothelin and undergoes subsequent internalization. The binding properties are not altered by the presence of the mesothelin-binding CA125 (43) and are fully retained in the ADC BAY 94-9343. BAY 94-9343 is shown to be both potent and highly selective in killing mesothelin-expressing tumor cells, whereas the same dose range does not affect mesothelin-negative cells.

DM4, the tubulin-binding toxophore, mainly acts on proliferating cells and therefore provides further functional specificity to the ADC beyond the specific target-binding of the antibody moiety. Indeed, we and others (44) observed no cytotoxicity upon treatment of mesothelin-expressing primary mesothelial cells with low proliferation rates. In contrast, the bacterial immunotoxin PE38 in SS1P is not only highly immunogenic, preventing readministration, but is also toxic to all antigen-positive cells due to its mode of action (21). Whole animal imaging using a fluorescently labeled antibody that is selectively retained in antigen-positive tumors demonstrates target selectivity and tumor specificity of the anti-mesothelin antibody *in vivo*. Furthermore, treatment of mice, bearing either mesothelin-negative or mesothelin-positive tumors, with BAY 94-9343 or a nontargeted ADC control harboring the same linker toxophore, respectively, indicates that the target-independent antitumor effects are only minor when compared with the targeted activity of BAY 94-9343. The inferior target-independent *in vivo* effects of the control ADC at high doses are presumably

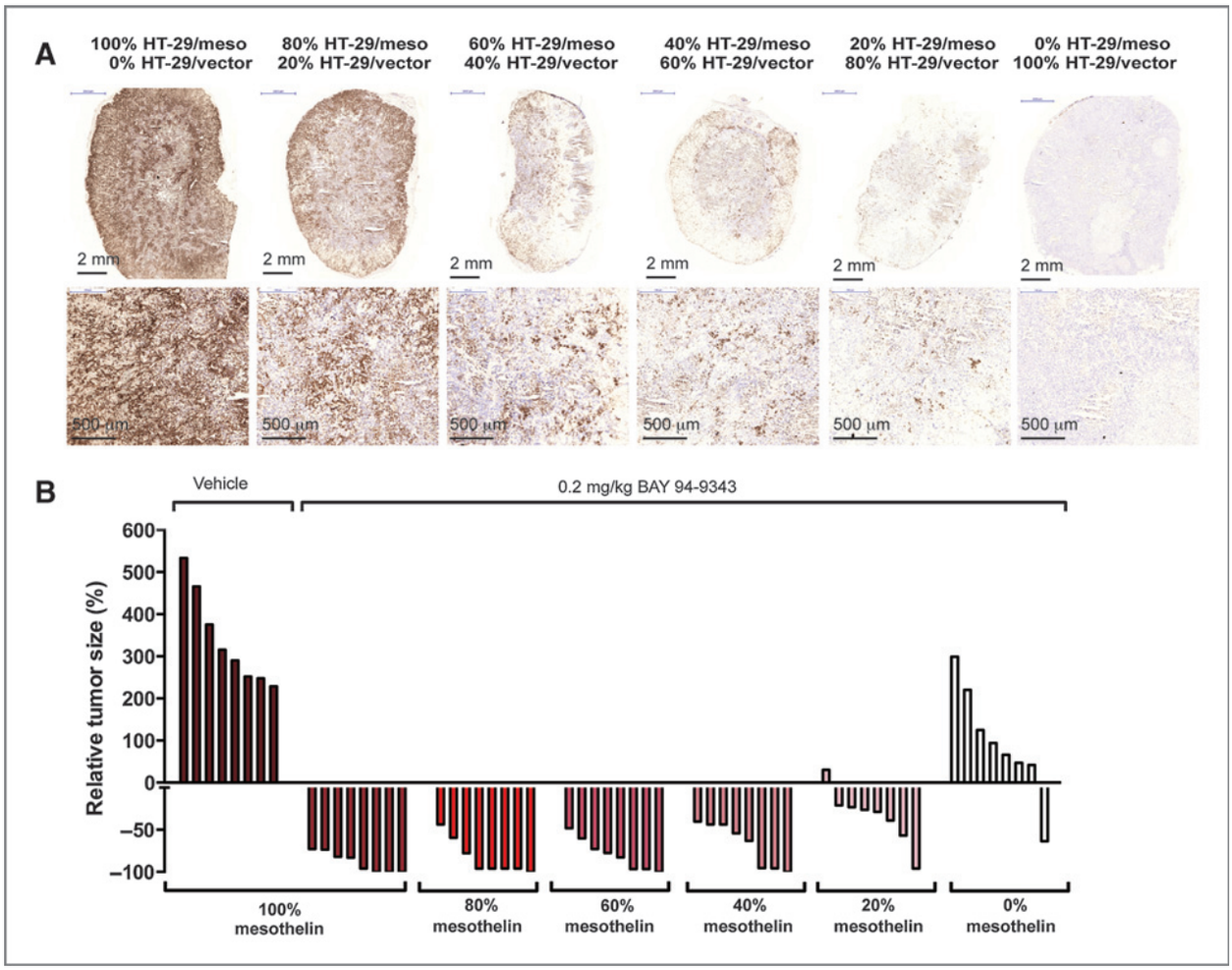

Figure 6. Titration of mesothelin-positive tumor cells *in vivo*. Different ratios of mesothelin- and vector-transfected HT-29 cells were subcutaneously transplanted into nude mice (randomized on day 6 to treatment and vehicle groups). A, immunohistochemical staining of mesothelin in vehicle-treated tumors. B, changes in tumor size from randomization until day 28 (the last time point at which the vehicle groups remained in the study). Each bar represents the change in tumor size during the study of an individual mouse. Positive bars represent growth and negative bars shrinkage of tumors as compared with tumor size at treatment start. The vehicle control was included in all the different study groups but the data are only shown for the group inoculated with 100% mesothelin-positive cells.

due to enhanced permeability and retention (EPR) in solid tumors. This phenomenon of passive drug targeting of tumors has been widely described for macromolecules and lipids (45).

Once BAY 94-9343 is bound and internalized by a tumor cell, degradation of the BAY 94-9343 disulfide-based linker releases a cell permeable toxophore metabolite with bystander killing potential (33). This bystander effect was demonstrated, for the first time *in vivo*, using a *xenograft* model with different proportions of mesothelin-positive and -negative cells within the inoculated tumors. BAY 94-9343 not only inhibited tumor growth, but also more importantly induced tumor regression even when only 20% of the cells within the tumor were mesothelin positive. This strongly suggests that, in addition to the EPR effect observed in the mesothelin-negative cells, the bystander effect contributes to the antitumor activity of BAY 94-9343. Similar results have been reported previously by Kovtun and colleagues (30).

In addition to the subcutaneous and orthotopic xenograft tumor models, we further demonstrated the dose-dependent therapeutic activity of BAY 94-9343 in patient-derived tumors that more closely mimic human tumor characteristics, such as heterogeneity. Treatment with BAY 94-9343 resulted in total eradication of established tumors with no tumor recurrence and was reproducible in several models over a long observational period, further indicating complete tumor cell elimination by the ADC. Importantly, the efficacy of BAY 94-9343 in pancreatic, ovarian, and mesothelioma cancer models was more pronounced as compared with the current respective standard-of-care treatments, suggesting that BAY 94-

9343 is a potential therapeutic option for patients with heavily pretreated and even resistant tumors.

Taken together, our preclinical results validate mesothelin as a cancer antigen for an ADC as a potential therapeutic approach. Future studies determining the threshold of mesothelin expression required to achieve efficient ADC-induced antitumor efficacy are essential. This information is crucial in developing companion diagnostics to stratify patient populations in clinical development. Currently, anetumab ravtansine (BAY 94-9343) is in phase I clinical evaluation about its safety, tolerability, pharmacokinetics, and pharmacodynamics (ClinicalTrials.gov Identifier: NCT01439152). The maximum tolerated dose of anetumab ravtansine will be assessed in several advanced solid tumors with high frequency of mesothelin expression.

Disclosure of Potential Conflicts of Interest

C. Kopitz has ownership interest in holding parts of the corresponding patent. A. Kahnert has ownership interest in shares and patent. No potential conflicts of interest were disclosed by the other authors.

Authors' Contributions

Conception and design: S. Golfier, C. Kopitz, A. Kahnert, I. Heisler, B. Stelte-Ludwig, A. Harrenga, B. Müller-Tiemann, B. Kreft

Development of methodology: S. Golfier, C. Kopitz, I. Heisler, B. Stelte-Ludwig, L. Linden, A. Harrenga, P. Hauff, F.-D. Scholle, B. Müller-Tiemann, S. Bruder

Acquisition of data (provided animals, acquired and managed patients, provided facilities, etc.): S. Golfier, C. Kopitz, I. Heisler, C.A. Schatz, B. Stelte-Ludwig, A. Mayer-Bartschmid, K. Unterschemmann, A. Harrenga, P. Hauff, F.-D. Scholle, B. Müller-Tiemann, S. Bruder

Analysis and interpretation of data (e.g., statistical analysis, biostatistics, computational analysis): S. Golfier, C. Kopitz, A. Kahnert, I. Heisler, B. Stelte-Ludwig, A. Harrenga, P. Hauff, F.-D. Scholle, B. Müller-Tiemann, B. Kreft, S. Bruder

Writing, review, and/or revision of the manuscript: S. Golfier, C. Kopitz, A. Kahnert, I. Heisler, B. Stelte-Ludwig, B. Kreft

Administrative, technical, or material support (i.e., reporting or organizing data, constructing databases): I. Heisler, B. Müller-Tiemann

Study supervision: B. Müller-Tiemann, B. Kreft, K. Ziegelbauer

Acknowledgments

The authors thank Stephanie Ernesti, Karola Henschel, Katrin Jänsch, Sabrina Leppin, and Bianka Timpner for excellent technical assistance, Aurexel Ltd. (www.aurexel.com) for editorial support funded by Bayer HealthCare Pharmaceuticals, ImmunoGen Inc., for their support and valued advice about maytansinoid-ADCs, and Lauren Clancy (of ImmunoGen) for skillful preparation of the conjugates studied herein.

The costs of publication of this article were defrayed in part by the payment of page charges. This article must therefore be hereby marked *advertisement* in accordance with 18 U.S.C. Section 1734 solely to indicate this fact.

Received October 25, 2013; revised March 24, 2014; accepted March 26, 2014; published OnlineFirst April 8, 2014.

References

1. Hassan R, Bera T, Pastan I. Mesothelin: a new target for immunotherapy. Clin Cancer Res 2004;10:3937–42.
2. Hassan R, Ho M. Mesothelin targeted cancer immunotherapy. Eur J Cancer 2008;44:46–53.
3. Argani P, Iacobuzio-Donahue C, Ryu B, Rosty C, Goggins M, Wilentz RE, et al. Mesothelin is overexpressed in the vast majority of ductal adenocarcinomas of the pancreas: identification of a new pancreatic cancer marker by serial analysis of gene expression (SAGE). Clin Cancer Res 2001;7:3862–8.
4. Baba K, Ishigami S, Arigami T, Uenosono Y, Okumura H, Matsumoto M, et al. Mesothelin expression correlates with prolonged patient survival in gastric cancer. J Surg Oncol 2012;105:195–9.
5. Hassan R, Kreitman RJ, Pastan I, Willingham MC. Localization of mesothelin in epithelial ovarian cancer. Appl Immunohistochem Mol Morphol 2005;13:243–7.
6. Ordonez NG. Application of mesothelin immunostaining in tumor diagnosis. Am J Surg Pathol 2003;27:1418–28.
7. Ordonez NG. Value of mesothelin immunostaining in the diagnosis of mesothelioma. Mod Pathol 2003;16:192–7.
8. Tchou J, Wang LC, Selven B, Zhang H, Conejo-Garcia J, Borghaei H, et al. Mesothelin, a novel immunotherapy target for triple negative breast cancer. Breast Cancer Res Treat 2012;133:799–804.
9. Chang K, Pastan I. Molecular cloning of mesothelin, a differentiation antigen present on mesothelium, mesotheliomas, and ovarian cancers. Proc Natl Acad Sci U S A 1996;93:136–40.
10. Bera TK, Pastan I. Mesothelin is not required for normal mouse development or reproduction. Mol Cell Biol 2000;20:2902–6.
11. Gubbels JA, Belisle J, Onda M, Rancourt C, Migneault M, Ho M, et al. Mesothelin-MUC16 binding is a high affinity, N-glycan dependent interaction that facilitates peritoneal metastasis of ovarian tumors. Mol Cancer 2006;5:50.
12. Rump A, Morikawa Y, Tanaka M, Minami S, Umesaki N, Takeuchi M, et al. Binding of ovarian cancer antigen CA125/MUC16 to mesothelin mediates cell adhesion. J Biol Chem 2004;279:9190–8.
13. Chang MC, Chen CA, Chen PJ, Chiang YC, Chen YL, Mao TL, et al. Mesothelin enhances invasion of ovarian cancer by inducing MMP-7 through MAPK/ERK and JNK pathways. Biochem J 2012;442:293–302.
14. Servais EL, Colovos C, Rodriguez L, Bograd AJ, Nitadori J, Sima C, et al. Mesothelin overexpression promotes mesothelioma cell invasion and mmp-9 secretion in an orthotopic mouse model and in epithelioid pleural mesothelioma patients. Clin Cancer Res 2012;18:2478–89.
15. Bharadwaj U, Marin-Muller C, Li M, Chen C, Yao Q. Mesothelin confers pancreatic cancer cell resistance to TNF-alpha-induced apoptosis through Akt/PI3K/NF-kappaB activation and IL-6/Mcl-1 overexpression. Mol Cancer 2011;10:106.
16. Bharadwaj U, Marin-Muller C, Li M, Chen C, Yao Q. Mesothelin overexpression promotes autocrine IL-6/sIL-6R trans-signaling to stimulate pancreatic cancer cell proliferation. Carcinogenesis 2011;32:1013–24.
17. Kelly RJ, Sharon E, Pastan I, Hassan R. Mesothelin-targeted agents in clinical trials and in preclinical development. Mol Cancer Ther 2012;11:517–25.
18. Hassan R, Cohen SJ, Phillips M, Pastan I, Sharon E, Kelly RJ, et al. Phase I clinical trial of the chimeric anti-mesothelin monoclonal antibody MORAb-009 in patients with mesothelin-expressing cancers. Clin Cancer Res 2010;16:6132–8.
19. Hassan R, Sharon E, Schuler B, Mallory Y, Zhang J, Ling A, et al. Antitumor activity of SS1P with pemetrexed and cisplatin for front-line treatment of pleural mesothelioma and utility of serum mesothelin as a marker of tumor response. J Clin Oncol 29: 2011 (suppl; abstr 7026).
20. Le DT, Brockstedt DG, Nir-Paz R, Hampl J, Mathur S, Nemunaitis J, et al. A live-attenuated Listeria vaccine (ANZ-100) and a live-attenuated Listeria vaccine expressing mesothelin (CRS-207) for advanced cancers: phase I studies of safety and immune induction. Clin Cancer Res 2012;18:858–68.
21. Hassan R, Bullock S, Premkumar A, Kreitman RJ, Kindler H, Willingham MC, et al. Phase I study of SS1P, a recombinant anti-mesothelin immunotoxin given as a bolus I.V. infusion to patients with mesothelin-expressing mesothelioma, ovarian, and pancreatic cancers. Clin Cancer Res 2007;13:5144–9.
22. Weldon JE, Xiang L, Zhang J, Beers R, Walker DA, Onda M, et al. A recombinant immunotoxin against the tumor-associated antigen mesothelin reengineered for high activity, low off-target toxicity, and reduced antigenicity. Mol Cancer Ther 2012; 12:48–57.

23. Pastan I, Hassan R, Fitzgerald DJ, Kreitman RJ. Immunotoxin therapy of cancer. Nat Rev Cancer 2006;6:559–65.
24. Blanc V, Bousseau A, Caron A, Carrez C, Lutz RJ, Lambert JM. SAR3419: an anti-CD19-Maytansinoid Immunoconjugate for the treatment of B-cell malignancies. Clin Cancer Res 2011;17:6448–58.
25. Katz J, Janik JE, Younes A. Brentuximab Vedotin (SGN-35). Clin Cancer Res 2011;17:6428–36.
26. Younes A, Gopal AK, Smith SE, Ansell SM, Rosenblatt JD, Savage KJ, et al. Results of a Pivotal Phase II Study of Brentuximab Vedotin for Patients With Relapsed or Refractory Hodgkin's Lymphoma. J Clin Oncol 2012;30:2183–9.
27. Burris HA III, Rugo HS, Vukelja SJ, Vogel CL, Borson RA, Limentani S, et al. Phase II study of the antibody drug conjugate trastuzumab-DM1 for the treatment of human epidermal growth factor receptor 2 (HER2)-positive breast cancer after prior HER2-directed therapy. J Clin Oncol 2011;29:398–405.
28. LoRusso PM, Weiss D, Guardino E, Girish S, Sliwkowski MX. Trastuzumab emtansine: a unique antibody-drug conjugate in development for human epidermal growth factor receptor 2-positive cancer. Clin Cancer Res 2011;17:6437–47.
29. Krop IE, LoRusso P, Miller KD, Modi S, Yardley D, Rodriguez G, et al. A phase II study of trastuzumab emtansine in patients with human epidermal growth factor receptor 2-positive metastatic breast cancer who were previously treated with trastuzumab, lapatinib, an anthracycline, a taxane, and capecitabine. J Clin Oncol 2012;30:3234–41.
30. Kovtun YV, Audette CA, Ye Y, Xie H, Ruberti MF, Phinney SJ, et al. Antibody-drug conjugates designed to eradicate tumors with homogeneous and heterogeneous expression of the target antigen. Cancer Res 2006;66:3214–21.
31. Miyamori H, Takino T, Kobayashi Y, Tokai H, Itoh Y, Seiki M, et al. Claudin promotes activation of pro-matrix metalloproteinase-2 mediated by membrane-type matrix metalloproteinases. J Biol Chem 2001;276:28204–11.
32. Chari RV, Martell BA, Gross JL, Cook SB, Shah SA, Blattler WA, et al. Immunoconjugates containing novel maytansinoids: promising anticancer drugs. Cancer Res 1992;52:127–31.
33. Erickson HK, Park PU, Widdison WC, Kovtun YV, Garrett LM, Hoffman K, et al. Antibody-maytansinoid conjugates are activated in targeted cancer cells by lysosomal degradation and linker-dependent intracellular processing. Cancer Res 2006;66:4426–33.
34. Widdison WC, Wilhelm SD, Cavanagh EE, Whiteman KR, Leece BA, Kovtun Y, et al. Semisynthetic maytansine analogues for the targeted treatment of cancer. J Med Chem 2006;49:4392–408.
35. Hamblett KJ, Senter PD, Chace DF, Sun MM, Lenox J, Cerveny CG, et al. Effects of drug loading on the antitumor activity of a monoclonal antibody drug conjugate. Clin Cancer Res 2004;10:7063–70.
36. Perlitz C, Licha K, Scholle FD, Ebert B, Bahner M, Hauff P, et al. Comparison of two tricarbocyanine-based dyes for fluorescence optical imaging. J Fluoresc 2005;15:443–54.
37. Tentler JJ, Tan AC, Weekes CD, Jimeno A, Leong S, Pitts TM, et al. Patient-derived tumour xenografts as models for oncology drug development. Nat Rev Clin Oncol 2012;9:338–50.
38. Ho M, Feng M, Fisher RJ, Rader C, Pastan I. A novel high-affinity human monoclonal antibody to mesothelin. Int J Cancer 2011;128:2020–30.
39. Ostendorp R, Frisch C, Urban M. Generation, engineering and production of human antibodies using HuCAL. Springer. Antibodies 2011;2:13–52.
40. Murphy RF, Powers S, Cantor CR. Endosome pH measured in single cells by dual fluorescence flow cytometry: rapid acidification of insulin to pH 6. J Cell Biol 1984;98:1757–62.
41. Marshall J. Clinical implications of the mechanism of epidermal growth factor receptor inhibitors. Cancer 2006;107:1207–18.
42. Spector NL, Blackwell KL. Understanding the mechanisms behind trastuzumab therapy for human epidermal growth factor receptor 2-positive breast cancer. J Clin Oncol 2009;27:5838–47.
43. Kahnert A, Light D, Schneider D, Parry R, Satozawa N, Heitner T, et al. Anti-mesothelin antibodies and uses thereof. PCT/EP2008/009756. 2008 Nov 19.
44. Leard LE, Broaddus VC. Mesothelial cell proliferation and apoptosis. Respirology 2004;9:292–9.
45. Maeda H. The enhanced permeability and retention (EPR) effect in tumor vasculature: the key role of tumor-selective macromolecular drug targeting. Adv Enzyme Regul 2001;41:189–207.